CONSTRAINING THE FORMATION OF PALLASITE METEORITES WITH COUPLED MULTI-SCALE MODELLING. M. Murphy Quinlan[1]*, A. M. Walker[2], C. J. Davies[1], J. E. Mound[1], T. Müller[3], J. Harvey[1] [1]School of Earth and Environment, University of Leeds, Leeds, U.K. [2]Department of Earth Sciences, University of Oxford, Oxford, U.K. [3]Geoscience Center, Georg-August-University Göttingen, Göttingen, Germany. *Email: eememq@leeds.ac.uk

Introduction: Pallasite meteorites are samples of differentiated planetesimals, comprising a mixture of Fe-Ni metal and olivine. A wide range of formation hypotheses have been suggested in the literature to explain the proximity of mantle and core material in Pallasite Main Group (PMG) samples, including fractional melting and differentiation in a single body [1], impact mixing [2], ferrovolcanism [3], or a combination of these processes [4]. Pallasites record slow cooling (~K/Myr) at low temperatures in the metal phase and orders of magnitude faster cooling at higher temperatures in the silicate phase [5]; this contrast has been difficult to reconcile in numerical models of a single parent body. We model the parent body by assuming intrusion of metal into the mantle, either from a metallic bolide or through entrainment of core material from within the body, and find intrusion depths and parent body geometries that agree with both cooling rates without the addition of a thick post-impact regolith. Understanding the formation environment of pallasite meteorites would provide an insight into the deep interior of planetary building blocks and inform our understanding of planet-building processes in our Solar System.

Cooling rates: Pallasite meteorites record thermal processes and cooling rates on different spatial and temporal scales: slow, planetary cooling is recorded in the metal region by Ni diffusion in Widmanstätten texture [6], while cooling on geologically short timescales is suggested by the preservation of easily-erased original igneous zoning [7] and presence of diffusion-related gradients [5, 8, 9, 10] in olivine. The degree of rounding of olivine [11, 12, 13, 14] adds another temporal constraint. These short-timescale processes may be related to the injection of molten metal into a cooler silicate mantle and subsequent rapid cooling.

Methods: We aim to reconcile these two different timescales and build a model of the pallasite parent body that reproduces evidence from both the metal and silicate portion of pallasite samples. We couple the planetesimal-scale model described in Murphy Quinlan et al., 2021 [15] with a new regional-scale 3D metal-olivine mixing model (Fig. 1) to constrain the environment of pallasite formation and track the thermal evolution of the region of olivine and metal mixing within the pallasite parent body.

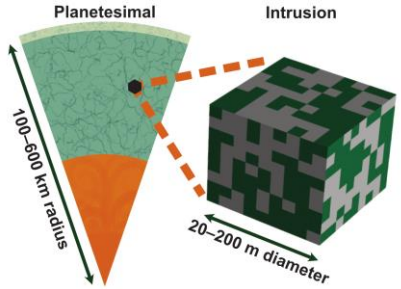

Figure 1. *Cartoon of coupled models, not to scale.*

Numerical model: We use the open-source Python package Pytesimal [16] to model conductively cooling planetesimals and choose a selection of parent body geometries which are compatible with metal cooling rates recorded in pallasite meteorites [15, 17, 18]. We then use the resulting mantle temperature distributions as wall-rock temperature inputs when modelling the intrusion of hot metal into the planetesimal mantle.

We apply the semi-implicit Crank-Nicolson scheme [19] with the Fractional Step Method for 3D extension [20, 21] to model the temperature evolution of a metallic intrusion in an olivine mantle. We incorporate spatially varying diffusivity [22] to capture the material property contrast between the mantle and mixed olivine and metal region. Far from the intrusion, a zero-flux boundary condition is imposed, which allows the mixed-phase intrusion and surrounding country rock to evolve without an artificially imposed fixed temperature condition [23, Fig. 2].

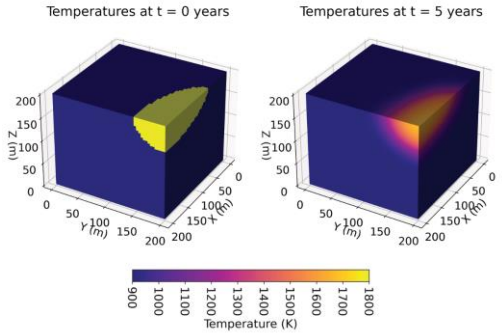

Figure 2. *Temperatures within the intrusion region at times t = 0 and t = 5 years.*

The pallasite mixing region diverges from simple igneous intrusion models when the observed texture of samples is considered: olivine forms a solid interconnected framework that is infiltrated by molten

metal (Fig. 1). We model the mixed region macroscopically by taking appropriate weighted averages of the olivine and metal material properties. We capture the latent heat of crystallisation of the metal during freezing using the apparent heat capacity method and track the solidification front via the metal solidus isotherm [24]. Our 3D model is constrained to a choice of temperature-dependent conductivity that results in a small non-linear term.

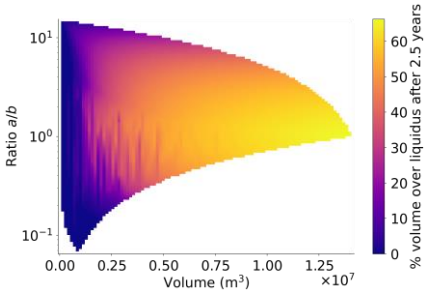

Figure 3. *Temperatures within the intrusion region as a percentage by volume of an ellipsoidal intrusion, with intrusion volume in m3 on the x-axis and the ratio of unique (a) to non-unique (b) axes of a uniaxial ellipsoid on the y-axis. Note that coarse sampling of the model parameter space has introduced some artefacts in the contouring.*

Preliminary results: We find that aspect ratio is a strongly controlling factor on the cooling rate of metal intrusions into planetesimal mantles; sheet and pipe morphologies cool more rapidly than equal volume spherical magma chambers (Fig. 3). Surrounding mantle temperature, controlled by planetesimal radius and core size, depth in the planetesimal mantle, and time after magma ocean solidification, controls how quickly the molten metal cools and crystallizes after infiltrating the olivine, allowing us to discriminate between different planetesimal geometries. We verify that slow, low-temperature metal cooling rates do record the overall planetesimal mantle cooling (and so can be used to estimate the residence depth of pallasite material within the parent body), instead of recording the slow cooling of an intrusion towards the ambient mantle temperature. In preliminary model runs, we reproduce the cooling rates suggested to explain diffusional gradients in olivine rims [8, and others], and find intrusion morphologies that cool quickly enough to preserve original igneous zoning in olivine, and slowly enough to produce rounding in small olivine grains, for example in a 100 m radius elliptical intrusion in a 250 km radius parent body. By design, these intrusion geometries also agree with metallographic cooling rates and the associated depth of residence within the parent body. We are working towards systematically sampling the parameter space to produce a range of planetesimal geometries, intrusion depths and intrusion geometries that simultaneously reproduce the available measured constraints.

Conclusions: Models of the pallasite parent body and hypotheses to describe their formation must agree with the evidence in samples, including the slow, low-temperature cooling rates recorded in the FeNi metal and the high-temperature, rapid cooling rates implied by olivine geochemistry and morphology. We couple a planetesimal-scale model with a regional metal-olivine mixing model to investigate which planetesimal geometries simultaneously meet the constraints imposed by the metal cooling rates and olivine cooling rates. Our model of the intrusion region combines novel numerical methods to investigate this porous medium phase-change problem in 3D. We test the sensitivity of our model to the input parameters and find a range of metal intrusion morphologies that satisfy observed constraints in pallasite meteorites.

[1] J. S. Boesenberg et al. (2012) Geochim. et Cosmochim. Acta, 89, 134–158. [2] J. A. Tarduno et al. (2012) Sci., 338, 939–942. [3] B. C. Johnson et al. (2019), Nat. Astro., 4, 41–44. [4] S. J. McKibbin, et al. (2019), Meteorit. Planet. Sci. 54, 2814–2844. [5] W. Hsu (2003), Meteorit. Planet. Sci. 38, 1217–1241. [6] J. Yang et al. (2010), Geochim. et Cosmochim. Acta 74, 4471–4492. [7] S. M. Chernonozhkin et al. (2021), Chem. Geo. 562, 119996. [8] M. Miyamoto (1997), JGR, 102, 21613–21618. [9] M. Miyamoto et al. (2004), Ann. Met. Soc. LXVII, 5119. [10] T. Tomiyama and G. Huss (2006), LPS XXXVII, 1–2. [11] K. Saiki et al. (2003), Meteorit. Planet. Sci. 38, 427–444. [12] G. F. Solferino et al. (2015) Geochim. et Cosmochim. Acta, 162, 259–275. [13] G. F. Solferino and G. J. Golabek (2018), EPSL, 504, 38–52. [14] N. P. Walte et al. (2020) EPSL, 546, 116419. [15] M. Murphy Quinlan et al. (2021), JGR:P, 126. [16] M. Murphy Quinlan et al. (2021) Pytesimal: v2.0.0, http://pytesimal.rtfd.io/ [17] J. F. Bryson et al. (2015), Nat., 517, 472–475. [18] C. I. O. Nichols et al. (2021), JGR:P 126. [19] J. Crank and P. Nicolson (1947), Math. Proc. Cambridge Philos. Soc., 43, 50–67. [20] W. Cen et al. (2016), AIP Adv., 6, 095305. [21] N. N. Yanenko, The Method of Fractional Steps, Springer Berlin Heidelberg, 1971. [22] M. Bengfort et al. (2018), Eco. Com., 34, 134–138. [23] C. Annen (2017), Front. in Earth Sci. 5, 82. [24] D. Mottaghy and V. Rath (2006), GJI, 164, 236–245.